Front. Environ. Sci. Eng. 2023, 17(3): 33
https://doi.org/10.1007/s11783-023-1633-0

RESEARCH ARTICLE

A pyrazine based metal-organic framework for selective removal of copper from strongly acidic solutions

Jiachuang Shao[1], Penghui Shao (✉)[1], Mingming Peng[1], Min Li[2], Ziwei Yao[1], Xiuqin Xiong[1], Caiting Qiu[1], Yufan Zheng[1], Liming Yang[1], Xubiao Luo (✉)[1]

1 Key Laboratory of Jiangxi Province for Persistent Pollutants Control and Resources Recycle, National-Local Joint Engineering Research Center of Heavy Metals Pollutants Control and Resource utilization, Nanchang Hangkong University, Nanchang 330063, China
2 Department of Chemical Engineering, Chongqing University of Science and Technology, Chongqing 401331, China

HIGHLIGHTS

- pz-UiO-66 was synthesized facilely by a solvothermal method.
- Efficient capture of copper from highly acidic solution was achieved by pz-UiO-66.
- pz-UiO-66 exhibited excellent selectivity and capacity for copper capture.
- Pyrazine-N in pz-UiO-66 was shown to be the dominant adsorption site.

ARTICLE INFO

Article history:
Received 17 July 2022
Revised 27 August 2022
Accepted 29 August 2022
Available online 14 October 2022

Keywords:
Pyrazine
Metal-organic frameworks
Copper removal
Strong acidity
High selectivity

GRAPHIC ABSTRACT

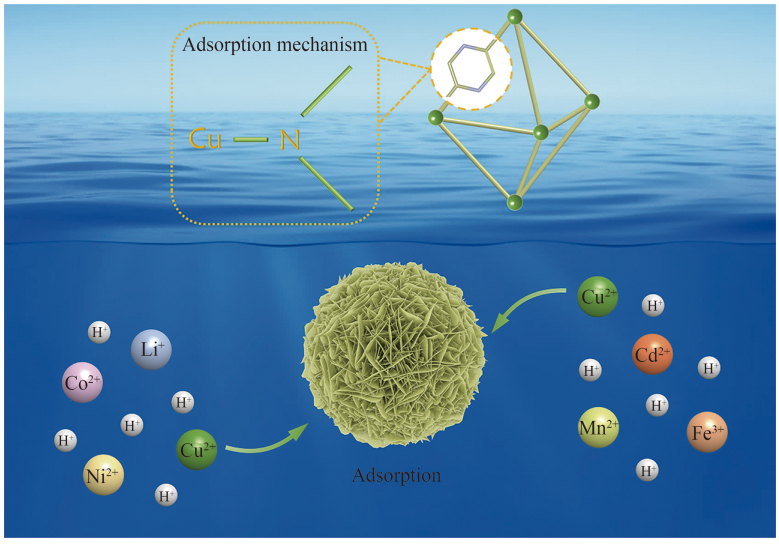

ABSTRACT

The selective capture of copper from strongly acidic solutions is of vital importance from the perspective of sustainable development and environmental protection. Metal organic frameworks (MOFs) have attracted the interest of many scholars for adsorption due to their fascinating physicochemical characteristics, including adjustable structure, strong stability and porosity. Herein, pz-UiO-66 containing a pyrazine structure is successfully synthesized for the efficient separation of copper from strongly acidic conditions. Selective copper removal at low pH values is accomplished by using this material that is not available in previously reported metal–organic frameworks. Furthermore, the material exhibits excellent adsorption capacity, with a theoretical maximum copper uptake of 247 mg/g. As proven by XPS and FT-IR analysis, the coordination of pyrazine nitrogen atoms with copper ions is the dominant adsorption mechanism of copper by pz-UiO-66. This work provides an opportunity for efficient and selective copper removal under strongly acidic conditions, and promises extensive application prospects for the removal of copper in the treatment for acid metallurgical wastewater.

1 Introduction

Copper, as a basic mineral element for human health, performs a critical role in enzyme synthesis and bone

✉ Corresponding authors
E-mails: luoxubiao@126.com (X. Luo);
penghui_shao@163.com (P. Shao)

development (Awual, 2019). However, the existence of excess copper is also related to many illnesses, such as cancer, Parkinsonian syndrome and Wilson's disease (Brady et al., 2014; Lee et al., 2016). Moreover, the World Health Organization (WHO) and Environmental Protection Agency (EPA) specify the upper limit concentrations of copper in drinking water of separately 2.0 and 1.3 mg/L (Fitzgerald, 1998). Given the ubiquity of copper in various industries and the negligence of copper-containing wastewater treatment in many industrial countries (Awual, 2019; Bui et al., 2020), maintaining a low concentration of copper ions in water has become the focus of global environmental governance. Therefore, seeking efficient technologies to remove copper from industrial wastewater is urgent. It is noteworthy that research on the selective separation of copper is also limited in the field of acid metallurgical wastewater treatment and urgently needs be improved. For example, the selective removal of copper from the anodic solution of nickel electrolysis before electrodeposition and the selective separation of copper from acid mine drainages have posed major challenges with respect to metallurgical industry wastewater and a more efficient approach is desired (Chen et al., 2013b; Park et al., 2019).

Various approaches have been applied to separate heavy metals from water media, including but not limited to ion exchange, chemical precipitation and electrochemical methods (Lin et al., 2017; Cao et al., 2019; Shao et al., 2020). Compared with other advanced technologies, adsorption has been proven to be a facile and high-efficiency approach for treating heavy metal ions due to the characteristics of its wide range of application, flexibility in operation, low energy consumption and low maintenance costs (Ai et al., 2016; Peng et al., 2018; Yao et al., 2022). Common adsorbent materials that are effective in removing copper include chelating resins (Chen et al., 2010; Chen et al., 2013a; Kuz'min and Kuz'min, 2014), carbon-based adsorbents (Demiral and Güngör, 2016), porous aromatic frameworks and metal-organic frameworks (MOFs) (Lee et al., 2016; Zhang et al., 2016). Several chelating resins have been investigated for removing copper, such as CEAD (Chen et al., 2013a), D001-PEI and Purolite S930 (Chen et al., 2010; Kuz'min and Kuz'min, 2014), however, all of them exhibit low adsorption capacities. A porous aromatic framework functionalized with thioether, PAF-1-SMe, was demonstrated to be selective and efficient in the extraction of copper from aqueous media as well as biological fluids, but it was specifically designed as a diagnostic tool to detect Wilson's disease (Lee et al., 2016). ZIF-8 was proven to be effective in capturing copper, with a reported uptake of 800 mg/g, establishing it as an effective copper adsorbent, although it was unstable in acidic solutions (Zhang et al., 2016). In general, most of the copper ion trapping materials investigated to date tend to suffer from certain defects, such as poor selectivity, insufficient capacity, or limited application at low pH; moreover, the synthesis of these materials usually uses expensive reagents that preclude large-scale production. To meet these challenges, one adsorbent with a high adsorption capacity, high selectivity to target ions, stability in strongly acidic solution and relatively fast adsorption kinetics is needed.

MOFs are new porous crystalline materials composed of metal centers connected by organic linkers. They have rich chemical properties and show promising application prospects in adsorption. Compared with traditional inorganic porous materials such as carbon nanotubes and silica, a significant drawback of MOFs is their lower stability. However, zirconium-based MOFs have drawn much attention owing to their outstanding stability compared with other common MOFs, in which strong Zr-O bonds impart remarkable chemical stability, mechanical stability as well as thermal stability (Cavka et al., 2008; Daliran et al., 2020; Zhang et al., 2021). These characteristics give Zr-MOFs excellent application prospects. Therefore, Zr-MOFs were chosen as an ideal candidate material to efficiently adsorb copper from aqueous solution under strongly acidic conditions. In addition, in strongly acidic solution, an extremely high hydrogen ion concentration will affect the ionization state of functional groups on the material, such as carboxyl groups and amino groups, thus affecting the adsorption capacity of the adsorbent. Pyrazine has two nitrogen donor atoms and is a weak base with a pKa value of 0.65. Even in strongly acidic solutions, the protonation of one nitrogen atom greatly reduces the electron cloud density of the other nitrogen atom, making it difficult to be protonated (Miniyar et al., 2013) and thus maintaining its coordination function with metal ions. Consequently, pyrazine nitrogen is used as the functional adsorption site in this study, which enables the functional groups on the material to remain effective at high hydrogen ion concentrations. In general, we take advantage of the highly oxygenophilic capability of Zr^{4+} and the stability of Zr-O, and consider the electron-withdrawing effect of pyrazine nitrogen atoms to design a material that can remain stable in strongly acidic solution and whose functional groups are not affected by protonation.

Herein, a Zr-MOF containing a pyrazine structure (pz-UiO-66) was successfully synthesized based on soft and hard acid-base (HSAB) theory and used for the removal of Cu^{2+} from strongly acidic wastewater. The successful synthesis of pz-UiO-66 was verified by XRD and FT-IR characterizations and the physical properties and morphology were explored by BET and SEM characterizations. Subsequently, the adsorption performance of pz-UiO-66 for Cu^{2+} under strongly acidic conditions and the adsorption selectivity for Cu^{2+} were investigated. Additionally, the mechanism of Cu^{2+} adsorption by pz-UiO-66 was further explored by XPS analysis.

2 Materials and methods

2.1 Chemicals

Pyrazine-2,5-dicarboxylic acid (H_2PzDC, 98 %), benzene-1,4-dicarboxylic acid (H_2BDC) and zirconium tetrachloride ($ZrCl_4$, 99.5 %) were supplied by J&K Scientific. Anhydrous ethanol (CH_3CH_2O, ⩾ 99.7 %) and N, N'-dimethylformamide (DMF, 99.5 %) were from Xilong Chemical. Cupric chloride ($CuCl_2{\cdot}2H_2O$), lithium chloride (LiCl), nickel (II) chloride hexahydrate ($NiCl_2{\cdot}6H_2O$), manganese chloride ($MnCl_2$), cobalt (II) chloride hexahydrate ($CoCl_2{\cdot}6H_2O$), cadmium dichloride ($CdCl_2{\cdot}2.5H_2O$) and iron chloride hexahydrate ($FeCl_3{\cdot}6H_2O$) were provided by Silong Chemical and Sinopharm Chemical Reagent. Each metal ion solution was prepared with deionized water which was purified through a Milli-Q water system (Bedford, USA).

2.2 Preparation of pz-UiO-66

The synthesis process of pz-UiO-66 is performed in Scheme 1. $ZrCl_4$ (0.233 g) and H_2PzDC (0.168 g) were dissolved in N,N'-dimethylformamide (DMF) (50 mL) and mixed under ultrasound until the mixture was clear. The obtained mixture was then poured into a 100 mL solvent bottle and placed in a 120 °C oven for 24 h. After cooling for a period of time, the crystallization product was filtered, followed by washing several times with DMF to remove the unreacted reagent, washed with ethanol several times to exchange DMF to ethanol, and dried at 60 °C. UiO-66 was prepared by replacing H_2PzDC with equal molar amounts of H_2BDC.

2.3 Characterization

The morphology characterization of the material was obtained through scanning electron microscopy (SEM) using a Nova Nano SEM450. The crystal structure of the adsorbent was measured based on X-ray diffraction (XRD) using a Bruker AXS with Cu Kα radiation, and recorded in the 2θ range from 5° to 60° at a scanning speed of 6°/min. Fourier transform infrared (FT-IR) spectrum of the adsorbents were collected at room temperature under dry conditions using a Bruker Vertex 70 FTIR (Ettlingen, Germany) spectrophotometer in the 400–4000 cm^{-1} region. The Brunner-Emmett-Teller (BET) surface areas and porosity of the adsorbents were performed using nitrogen adsorption and desorption at 77 K by a F-Sorb 3400 after evacuation at 100 °C for 12 h. X-ray photoelectron spectroscopy (XPS) was taken using a Kratos AXIS ULTRA DLD spectrometer to determine the elemental composition on the sample surface and explore the mechanism of adsorption. Thermogravimetric analysis (TGA) was conducted on the TGA Q600 SDT (New Castle, USA) in a nitrogen atmosphere, with the temperature ranging from 50 °C to 800 °C at a ramping rate of 6 °C/min. Atomic absorption spectrometry (AAS) was applied to determine metal ion concentrations using ContrAA 700 flame atomic absorption spectrophotometer from Analytik Jena, Germany.

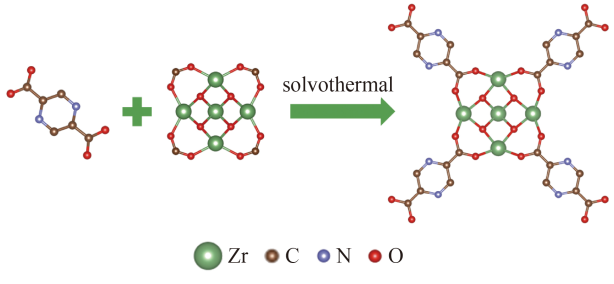

Scheme 1 Schematic diagram of preparation process of pz-UiO-66.

2.4 Effect of pH on adsorption

To investigate the effect of pH on the copper capture process, solutions comprised of 200 mg/L of Cu^{2+} were prepared with various pH values (1, 2, 3, 4). In the experiment, 20 mg pz-UiO-66 was added into conical flask containing 50 mL of metal ion solution, and the pH of water media was altered to the desired value by adding dilute sodium hydroxide or hydrochloric acid. Subsequently, the flask containing the solution to be adsorbed was placed in a shaker and reacted at a temperature of 298 K for 12 h at a speed of 180 r/min. After shaking, the solution was treated through a membrane filter of 0.22 μm, and the copper ions in the filtered solution were quantified by AAS. The adsorption performance (Q_e) for Cu^{2+} was estimated by Eq. (1):

$$Q_e = \frac{V(C_0 - C_e)}{m}, \quad (1)$$

where Q_e (mg/L) represents the quantity of adsorbed Cu^{2+}, C_0 and C_e (mg/L) are the original and balanced concentration of Cu^{2+}, separately, m (mg) is the weight of adsorbents, V (mL) is the volume of treated water media.

2.5 Selectivity experiment

The co-existed ion (Ni^{2+}, Co^{2+}, Mn^{2+}, Li^{+}, Fe^{3+}, Cd^{2+}) were carried out to explore the selectivity of pz-UiO-66 toward Cu^{2+}. The specific adsorption capacity of pz-UiO-66 for Cu^{2+} in a binary system comprised of Cu^{2+} and a coexisting ion was investigated firstly. Then, the selectivity of pz-UiO-66 was further analyzed in a multivariate system containing the seven ions mentioned above. All the ion concentrations were 5 mmol/L and the pH of solution was 1. Typically, 20 mg pz-UiO-66 and 50 mL of the above solution were mixed in a conical flask. After 12 h of continuous mixing, the solution was treated through a membrane filter of 0.22 μm, and the concentration of Cu^{2+} in the filtered solutions was determined by AAS.

To further illustrate the selectivity of pz-UiO-66 for Cu^{2+}, the experimental results from batch adsorption tests were used to calculate the distribution coefficient (K_d) for Cu^{2+} uptake using the Eq. (2) below:

$$K_d = 1000 \times \frac{(C_0 - C_e)V}{C_e m}, \quad (2)$$

where C_0 and C_e (mg/L) are separately the original and balanced concentration of Cu^{2+}.

2.6 Adsorption tests

The following tests, including adsorption kinetics and isothermal thermodynamics, were conducted at a pH of 1.

The adsorption kinetics of Cu^{2+} were examined at 25 °C by adding 200 mg of pz-UiO-66 into a 500 mL water sample with an initial Cu^{2+} concentrations of 200 mg/L and the solution were stirred at a constant rate. Equal amounts of the mixed solution were collected at predetermined intervals to confirm the concentration of remaining Cu^{2+} ions. The adsorption kinetic data were examined with the pseudo-first-order model (3) and pseudo-second-order model (4, 5) and the models were expressd as below:

$$\ln(Q_e - Q_t) = \ln Q_m - k_1 t, \quad (3)$$

$$\frac{t}{Q_t} = \frac{l}{k_2 Q_m^2} + \frac{t}{Q_m}, \quad (4)$$

$$h_0 = k_2 Q_e^2, \quad (5)$$

where Q_t (mg/g) is the quantity of adsorbate at t (min), Q_e (mg/g) is the copper uptake at equilibrium, and k_1 (min^{-1}), and k_2 (g/(mg·min)) and h_0 (mg/(g·min)) are the corresponding rate constants for the pseudo-first-order and second-order models.

Adsorption isotherm experiments were performed by oscillating a mixture containing 20 mg pz-UiO-66 and 50 mL aqueous Cu^{2+} solution with initial concentrations of Cu^{2+} ranging from 1 to 400 mg/L with a speed of 180 r/min for 12 h to achieve sorption equilibrium at 25 °C. The isothermal test data were processed with the Langmuir (6) and Freundlich (7) models:

$$Q_e = \frac{K_L Q_m C_e}{l + K_L C_e}, \quad (6)$$

$$Q_e = K_F C_e^{1/n}, \quad (7)$$

where C_e (mg/L) and Q_e (mg/g) separately correspond to the concentration of Cu^{2+} solution and the amount of adsorbed copper at equilibrium, Q_m (mg/g) represents the theoretical maximum adsorption capacity, K_L (L/mg) represents Langmuir constant, K_F ((mg/g)/ $(mg/L)^{1/n}$) and n are ascribed to Freundlich constant.

For the adsorption thermodynamic experiment, 20 mg pz-UiO-66 was added to a conical flask containing 50 mL Cu^{2+} solution at a concentration of 200 mg/L and then agitated in a shaker at 298 K, 308 K and 318 K. The thermodynamic parameters confirmed by the following Eqs. (8) and (9), namely, the standard Gibbs energy change (ΔG^0), enthalpy change (ΔH^0), and entropy change (ΔS^0), can provide insight into the energetic changes associated with the adsorption.

$$\ln K_d = \frac{\Delta S^0}{R} - \frac{\Delta H^0}{RT}, \quad (8)$$

$$\Delta G^0 = -RT \ln K_d, \quad (9)$$

where K_d (mL/g) is the distribution coefficient of the adsorbates, T (K) represents the temperature, and R is the gas constant, respectively.

3 Results and discussion

3.1 Characterization

The crystalline structure of pz-UiO-66 was characterized using powder X-ray diffraction (XRD). As displayed in Fig. 1(a), the as-synthesized material was highly crystalline and possessed the same structure as UiO-66, while slight peak broadening suggested lower crystallinity than the UiO-66 sample. The morphology and size of the prepared material were imaged through scanning electron microscopy (SEM), as depicted in Fig. S1. It could be observed in Fig. S1(c) that the pz-UiO-66 consisted of flower-like microspheres with rod-like petals and an average diameter of ≈ 4.5 μm. In addition, the uniform distribution of elements on the surface of the material was revealed by EDS analysis (Fig. S2). Fig. 1(b) showed that the FT-IR peaks of the MOF were mainly ascribed to the vibration of the ligand. In UiO-66, the peaks near 1650 cm^{-1} were caused by the stretching vibrations of C=O in carboxylic acid groups. The absorption bands at 1581 cm^{-1}, 1500 cm^{-1} and 1402 cm^{-1} belonged to the vibration absorption of the benzene ring skeleton and the peaks observed at 757 cm^{-1} were due to aromatic C-H bending vibrations. The peaks evolved at 1650 cm^{-1} and 750 cm^{-1} in pz-UiO-66 were consistent with those of UiO-66, and were related to the stretching vibrations of C=O bonds and aromatic C-H bonds, respectively. In addition, the peaks presented at 1487 cm^{-1}, 1433 cm^{-1} and 1381 cm^{-1} belonged to the stretching vibration absorption of the pyrazine ring skeleton, evidencing that pz-UiO-66 was successfully prepared.

Nitrogen adsorption-desorption isotherms was performed at 77 K to gain insight into the textural properties of pz-UiO-66. As depicted in Fig. 1(c), the isotherms of pz-UiO-66 conformed to the type II isotherm, indicating that pz-UiO-66 had a typical microporous structure. The BET specific surface area of pz-UiO-66 was 150 m^2/g, and the pore volume was 0.1943 cm^3/g. Moreover, the corresponding pore size was 0.4875 nm, and the size of the micropores allows the diffusion of copper ions within the

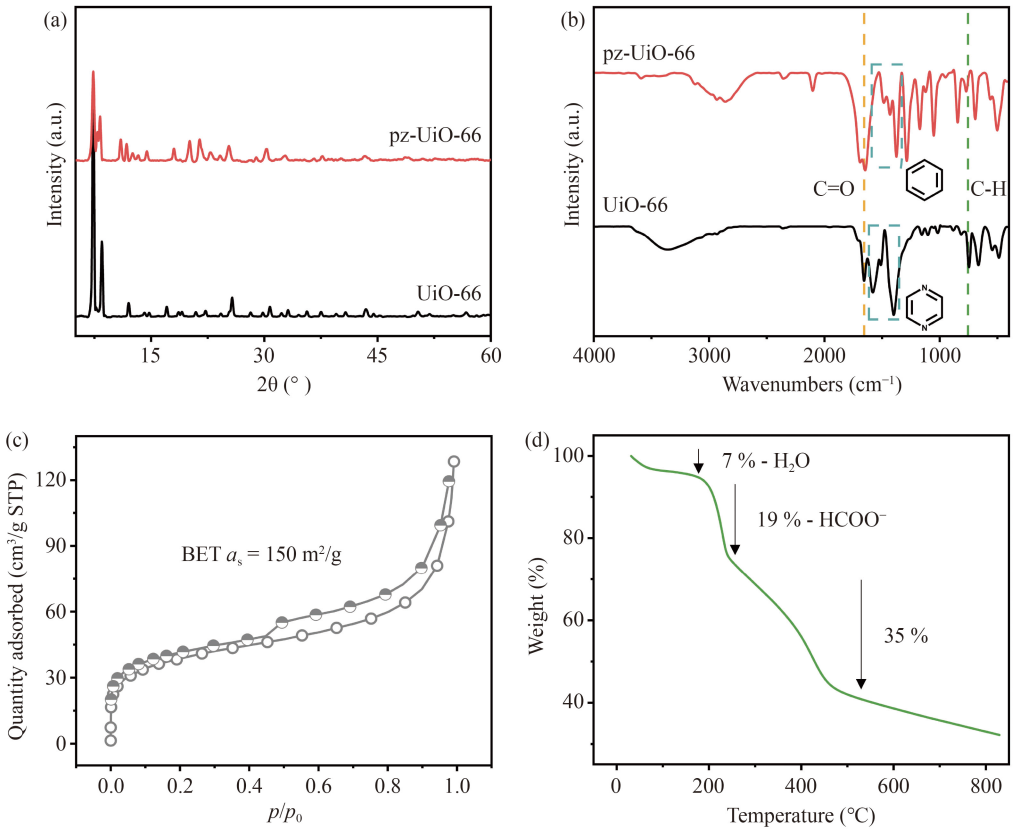

Fig. 1 XRD patterns (a) and FT-IR spectrum (b) of UiO-66 and pz-UiO-66, N_2 sorption isotherms (c) and TGA profiles (d) of pz-UiO-66.

material, bringing functional sites into contact with metal ions (Wang et al., 2019).

To assess the thermal behavior and structural integrity of pz-UiO-66, TGA-DSC curves were collected under a N_2 atmosphere and presented in Fig. 1(d). The initial loss of less than 10 % occurred at approximately 323 K, which was most likely ascribed to the loss of uncoordinated water. The next step of decomposition is then performed at 200 °C, likely due to ligand degradation. The final loss could be ascribed to the decomposition of the sample and the last temperature could be considered the upper limit of sample stability, indicating that pz-UiO-66 exhibited good thermal stability.

3.2 Effect of pH on adsorption

The pH value of the solution has a significant influence on the adsorption process of copper, because the acidity affects the ionization state of the adsorbent functional groups (Marcus, 1988; Xie et al., 2018). Therefore, the effect of pH on copper capture by pz-UiO-66 was studied. Since copper ions started to precipitate when the pH value was greater than 4.4, in order to prevent copper ions from forming hydroxide precipitates and affecting the adsorption process, the initial solution pH was selected in a suitable range from 1 to 4; within this range, Cu (II) exists in the form of Cu^{2+} in aqueous solution (Fig. S4). According to Fig. 2, the adsorption performance of pz-UiO-66 to Cu^{2+} was basically the same at pH 1–4, indicating that pz-UiO-66 possessed a strong independence for pH. It was worth noting that the adsorption capacity remained stable even at a strongly acidic pH of 1, which was attributed to the low pKa value of pyrazine in acidic solution, and the pyrazine nitrogen remained deprotonated, thus enabling pz-UiO-66 to adsorb Cu^{2+} ions in strongly acidic solutions.

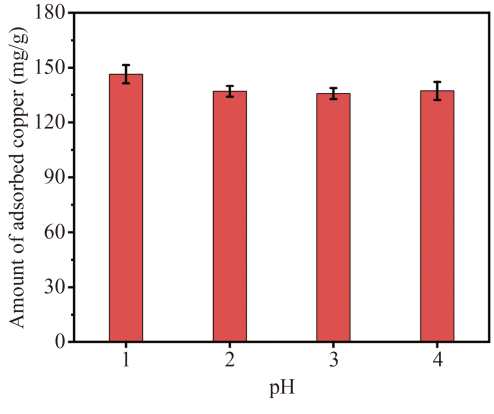

Fig. 2 Effect of pH on the adsorption of copper ions.

The adsorption process of copper on pz-UiO-66 was observed in Fig. 3(a), and the pz-UiO-66 underwent a color change at the room temperature. It could be seen that the color of pz-UiO-66 changed from off-white to green within the first 10 min during the copper adsorption process. The SEM image of pz-UiO-66 after adsorbing Cu^{2+} revealed that it retained a flower-like microsphere structure following 24 h of exposure to Cu^{2+}, while the microsphere surface became rougher due to the change of the more thickened petals (Fig. S1(f)). Furthermore, the elemental mapping images of pz-UiO-66 after capture of Cu^{2+} showed an even distribution of copper element on the surface of the adsorbent, manifesting that Cu^{2+} was successfully adsorbed on the material (Fig. 3(b)), and the EDS analysis results showed that the content of copper on pz-UiO-66 was slightly lower than the theoretical content, which might be attributed to the blockage of surface pores due to adsorption, resulting in more copper ions being unable to contact the adsorption site. In addition, the PXRD characterization revealed that pz-UiO-66 trans-

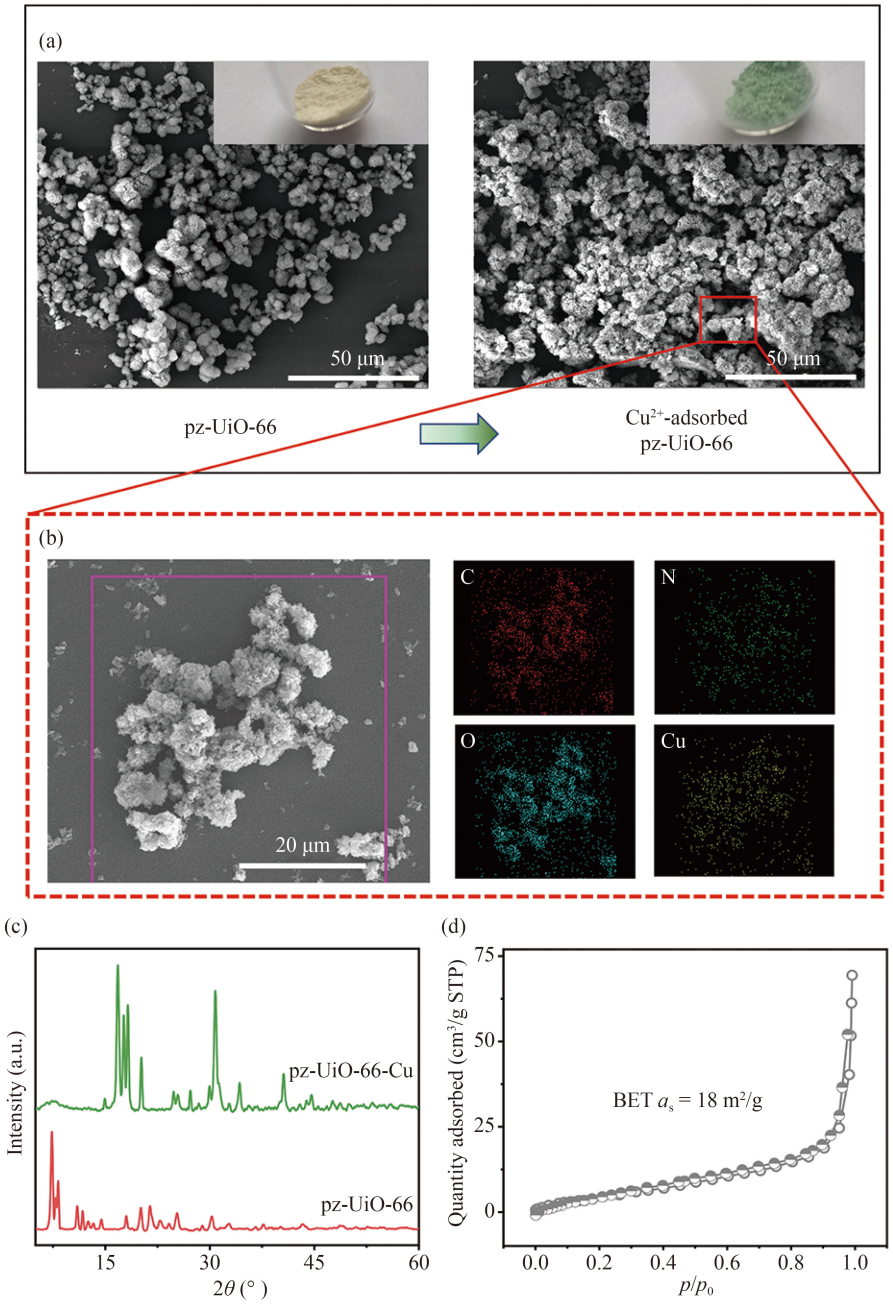

Fig. 3 Transformation of pz-UiO-66 after adsorption: (a) SEM images and optical properties of pz-UiO-66 and pz-UiO-66-Cu, (b) Extended scanning electron microscopy image and energy-dispersive X-ray spectroscopy analysis of pz-UiO-66-Cu, (c) PXRD data for pz-UiO-66 and pz-UiO-66-Cu, (d) N_2 sorption isotherms of pz-UiO-66-Cu.

mitted into a new crystal state after Cu^{2+} uptake, which might be due to the formation of new species (Fig. 3(c)). The N_2 adsorption-desorption isotherm of pz-UiO-66-Cu suggested that the BET surface area of the adsorbed material dropped sharply, which further proved the above speculation (Fig. 3(d)).

3.3 Selective adsorption

Given the complexity of actual water environments, the coexistence of metal ions might significantly influence the Cu^{2+} uptake efficacy. To validate the application potential of pz-UiO-66, selective adsorption of pz-UiO-66 was performed in solutions composed of Cu^{2+}, Li^{+}, Ni^{2+}, Co^{2+}, Fe^{3+}, Mn^{2+}, and Cd^{2+} ions. Notably, as illustrated in Fig. 4, the absorption of Cu^{2+} by pz-UiO-66 was much greater than that of other metal ions, or even did not adsorb other metal ions at all, which indicated that most of the binding sites on pz-UiO-66 were preferentially occupied by Cu^{2+} ions.

Subsequently, the copper distribution coefficient (K_d, mL/g) was calculated to further quantitatively assess the selectivity of pz-UiO-66 (Fig. 4(c)). In general, K_d represents the effectiveness of a sorbent in separating the target species and the selectivity of the sorbent for the species, in which $K_d > 5000$ is regarded as good and $K_d \geqslant 10^4$ is considered excellent. Notably, pz-UiO-66 exhibited K_d values as high as 10^4 at various concentrations of Cu^{2+}, indicating that pz-UiO-66 exhibited excellent selectivity for Cu^{2+} in strongly acidic solution, which would be beneficial to practical engineering applications.

The excellent selective adsorption of copper ions could be explained through hard-soft-acid-base (HSAB) theory and the stability of transition metal complexes. Pyrazine nitrogen as a borderline Lewis base, tends to form coordination bonds with borderline Lewis acids (Cu^{2+}, Ni^{2+}, Co^{2+}), rather than hard acids (Mn^{2+}, Li^{+}, Fe^{3+}) or soft acids (Cd^{2+}) (Xu et al., 2020). In addition, the specific adsorption of Cu^{2+} among transition metals (Cu^{2+}, Ni^{2+}, Co^{2+}) by pz-UiO-66 could be explained by the stability of transition metal complexes. Considering that copper complexes have higher stability than nickel and cobalt complexes, pyrazine nitrogen adsorption sites might preferentially coordinate with Cu^{2+} during solution adsorption (Irving and Williams, 1953). Further adsorption mechanisms are discussed in Section 3.6.

3.4 Adsorption isotherms

To further assess the adsorption performance of pz-UiO-66 for Cu^{2+}, the isothermal adsorption experiments were

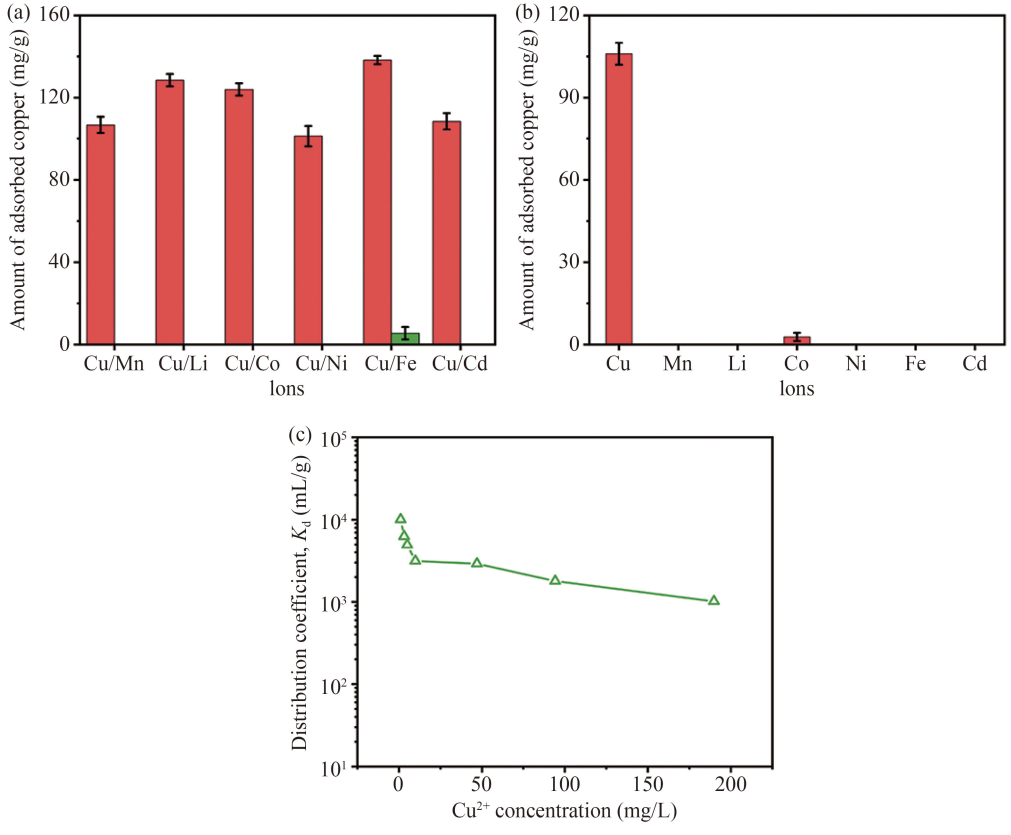

Fig. 4 Adsorption capacity of pz-UiO-66 for Cu^{2+} with coexisting Mn^{2+}, Li^{+}, Co^{2+}, Ni^{2+}, Fe^{3+} and Cd^{2+} in binary systems (a) and in a mixed solution composed of seven metal ions (b), distribution coefficients (c) of pz-UiO-66 with respect to Cu^{2+} concentration.

carried out over a wide range of copper concentrations, and the results are displayed in Fig. 5(a). The adsorption property of pz-UiO-66 for Cu^{2+} augmented as the initial concentration of Cu^{2+} rose, and reached a saturated uptake value of 147.5 mg/g at adsorption equilibrium. To better evaluate the adsorption performance of Cu^{2+} on pz-UiO-66, the Langmuir and Freundlich models were used to analyze the isotherm adsorption data at 25 °C (Yu et al., 2019), and the relevant parameters were tabulated in Table. S3. The Langmuir model was more suitable to express the copper capture process ascribed to its better correlation coefficient, suggesting that the adsorption on pz-UiO-66 was likely monolayer coverage. The fitting data indicated that the expected adsorption capacity of Cu^{2+} on pz-UiO-66 was 247 mg/g, slightly exceeding the actual capacity.

According to HSAB theory, N-functionalized adsorbents usually exhibit a certain adsorption capacity for Cu^{2+}, which is accomplished mainly through the formation of coordination bonds between nitrogen atoms and Cu^{2+} ions. Herein, the adsorption isotherms of most N-containing adsorbents for Cu^{2+} were analyzed. As shown in Fig. 5(b) and Table S4, most N-functionalized adsorbents, such as CEAD, D001-PEI and PLLA nanofibers, showed a maximum copper uptake of less than 2 mmol/g at pH 4-6, and almost no adsorption at pH values less than 2, which was owing to protonation of nitrogen atoms as the concentration of hydrogen ions increases, and the functional groups on the adsorbent could not capture Cu^{2+} under strongly acidic conditions. Although some pyridine-functionalized adsorbents exhibited a certain ability to remove Cu^{2+} at a pH of 1 or 2, the adsorption capacity of the adsorbents was still less than 0.5 mmol/g. The pz-UiO-66 in this work far outperformed most comparable reported adsorbents, exhibiting superior absorption performance in capturing Cu^{2+}. It had a fairly high adsorption capacity and was able to adapt to solutions with low pH values, which was quietly critical for the application of adsorbents for acid metallurgical wastewater treatment.

3.5 Adsorption kinetics and thermodynamics

To further explore the adsorption capacity of pz-UiO-66 for Cu^{2+}, the adsorption kinetics were performed at a strongly acidic pH of 1. As shown in Fig. 6(a), fast adsorption equilibrium on pz-UiO-66 was achieved within approximately 40 min due to the exposure of more pyrazine nitrogen atoms on the adsorbent surface, and after the rapid adsorption stage, the adsorption rate decreased as the nitrogen atoms used for adsorption tended to become saturated and the final adsorption saturation was achieved within 120 min. To further illustrate the dynamic behavior, pseudo-first- and pseudo-second-order models were applied to describe the kinetics data (Wang et al., 2022), as depicted in Fig. 6, as well as the fitting data listed in Table S5. Both linear fitting curves were displayed in Fig. 6, it was obvious that the pseudo-second-order curve had a better linear fitting compared with the other curve. In addition, from the kinetic parameters, the fitting of the pseudo-first-order model (R^2 = 0.972) reflected a lower correlation coefficient than that of the pseudo-second-order model (R^2 = 0.996), and the fitting value Q_m of the pseudo-second-order dynamics equation had a small deviation from the experimental data. This showed that the pseudo-second-order kinetic model was better than the first-order kinetic model for characterizing the copper capture process by pz-UiO-66, suggesting that chemical adsorption showed a dominant function in the adsorption process of Cu^{2+} by pz-UiO-66 (Choudhary et al., 2020).

To gain insight into the possible mechanisms involved in the removal process, the thermodynamics of adsorption were investigated. The adsorption data of pz-UiO-66 for copper at different temperatures were presented in Fig. 7 (a). The amount of adsorbed Cu^{2+} ions by pz-UiO-66 improved slightly with increasing temperature, as did the

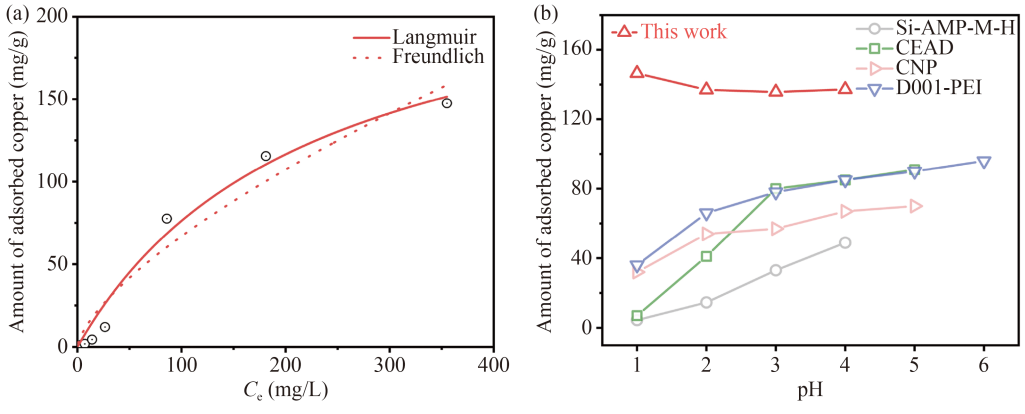

Fig. 5 Adsorption isotherms (a) for pz-UiO-66 fitted by Langmuir model and Freundlich model and comparative plot (b) of the effect of pH on copper adsorption for pz-UiO-66 and other copper ion sorbents.

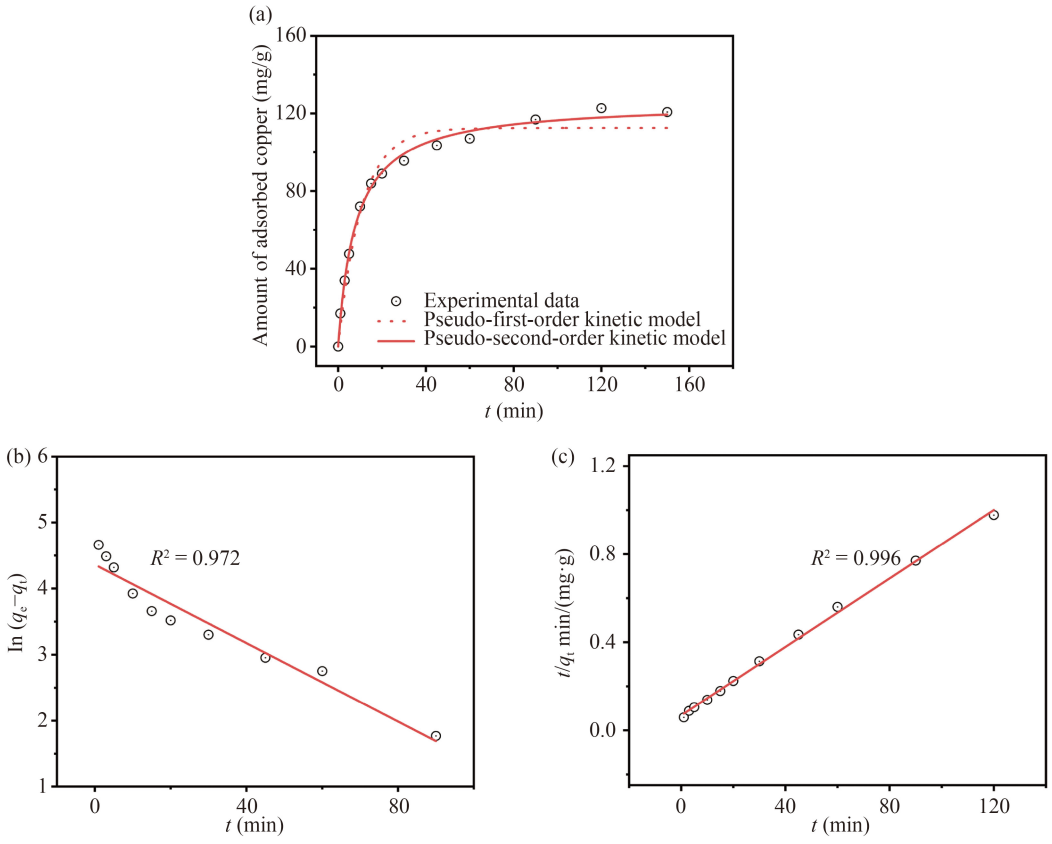

Fig. 6 Adsorption kinetics data and fitting curves (a), pseudo-first order (b) and pseudo-second order (c) plots of pz-UiO-66 for the adsorption of Cu^{2+}.

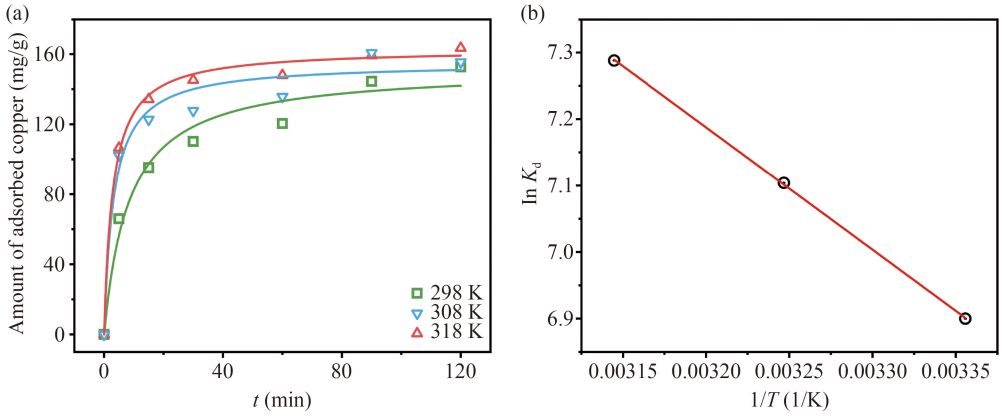

Fig. 7 Adsorption thermodynamics data (a) and plot of ln K_d *vs.* $1/T$ (b) for the adsorption of Cu^{2+} by pz-UiO-66.

adsorption rate, indicating that the effect of temperature on the adsorption performance was positively correlated. The van't Hoff graph, presented in Fig. 7(b), was plotted as ln K_d relative to $1/T$ to calculate the thermodynamic parameters and the results were summarized in Table. S6. The value of $\Delta H°$ for Cu^{2+} was positive, suggesting that the adsorption of Cu^{2+} by pz-UiO-66 was an endothermic process and driven by chemical reactions. The value of $\Delta S°$ was positive, implying that the randomness at the interface between the adsorbent and liquid was enhanced during the removal process. The negative value of ΔG^0 means that the reaction process could be spontaneous, which proved the feasibility of Cu^{2+} adsorption. Notably, the absolute value of ΔG^0 increased as the temperature rose. As previously reported, a more negative ΔG^0 is more conducive to a positive reaction (Jiang et al., 2019). Consequently, the adsorbent exhibited better adsorption performance for Cu^{2+} at 318 K.

3.6 Adsorption mechanism

To gain insight into the mechanisms leading to copper ion uptake in pz-UiO-66, FT-IR was applied to analyze the changes in the adsorption sites of pz-UiO-66 before and after the adsorption of copper ions, with the results presented in Fig. 8. It could be observed that the adsorption band at 2901 cm^{-1} belonged to stretching vibration of C-H on the pyrazine ring and the characteristic peaks near 1487 cm^{-1}, 1430 cm^{-1} and 1380 cm^{-1} were assigned to the skeletal vibration of pyrazine, all of which were associated with pz-UiO-66. It was noteworthy that the appearance of a new peak at 3410 cm^{-1} was ascribed to the stretching vibration of O-H after copper adsorption, which may be attributed to water molecules (Hosseinpournajjar et al., 2022). Moreover, the stretching vibration peak of pyrazine at 1432 cm^{-1} was significantly weakened and almost disappeared, which might be because pyrazine in pz-UiO-66 formed coordination bonds with copper, thus successfully adsorbing copper. The results showed that the process of pz-UiO-66 trapping copper ions was mainly through coordination interactions.

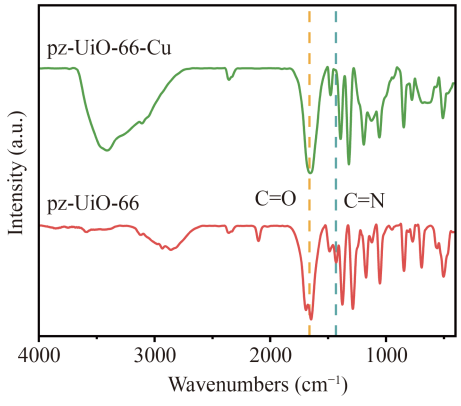

Fig. 8 FTIR spectrum of pz-UiO-66 before and after Cu^{2+} capture.

X-ray photoelectron spectroscopy (XPS) spectra were analyzed to further reveal the coordination interaction of pz-UiO-66 with copper ions, and the chemical composition of pz-UiO-66 before and after Cu^{2+} capture was determined. As displayed in Fig. 9(a), the corresponding regions of Zr 3d, O 1s, C 1s, and N 1s were clearly characterized in the measured scanning spectrum, and the presence of Cu 2p in the spectrogram after adsorption indicated that Cu^{2+} was successfully captured by pz-UiO-66, which was consistent with the SEM results. To be specific, the Cu 2p spectrum was analyzed, as presented in Fig. 9(b); the binding energies of 935.1 eV and 954.8 eV could be responsible for Cu $2p_{3/2}$ and Cu $2p_{1/2}$, respectively, and the satellite peaks of 944.2 eV and 963.4 eV could be ascribed to the presence of Cu^{2+} species (Feng et al., 2016). The Zr 3d spectra in Fig. 9(c) showed two obvious peaks at 184.95 eV and 182.55 eV during the adsorption process, indicative of Zr $3d_{3/2}$ and Zr $3d_{5/2}$, respectively, but these two peaks shifted to 185.2 eV and 182.8 eV after the adsorption of copper, and spectra of O 1s were shown in Fig. 9(d), giving a shift of M-O (M = metal) from 530 eV to 530.7 eV, manifesting that Zr nodes might also be involved in the adsorption process of

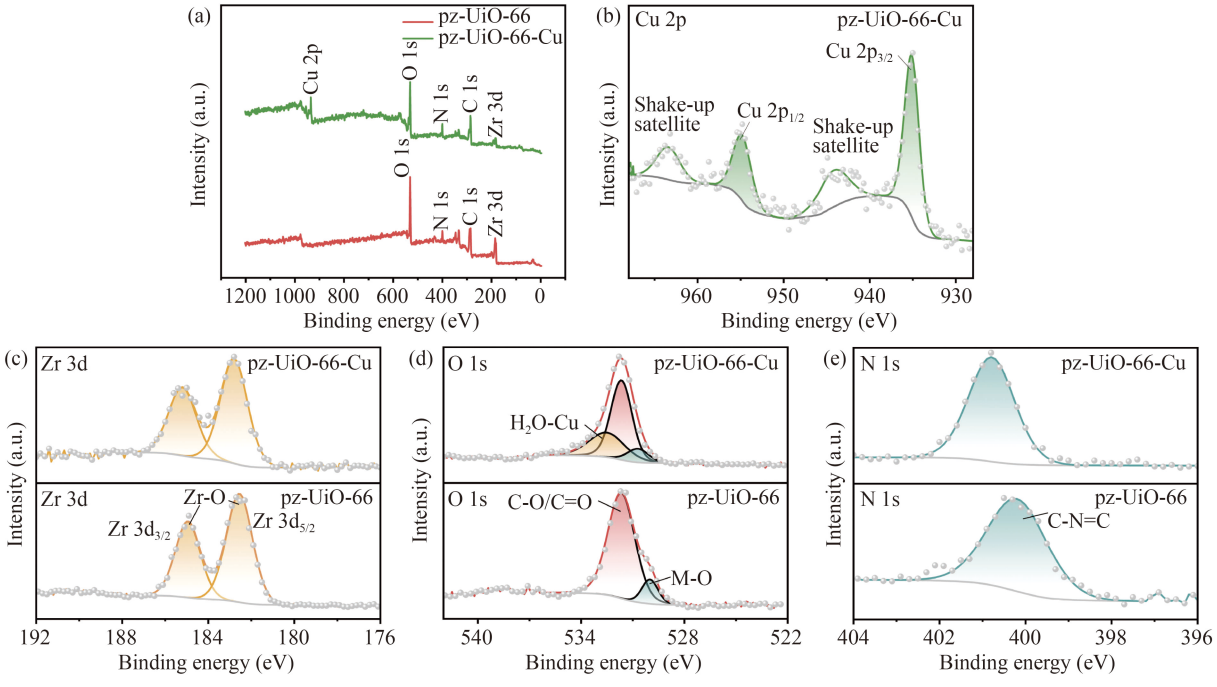

Fig. 9 XPS characterization of pz-UiO-66 before and after Cu^{2+} adsorption: (a) full spectrum, (b) Cu 2p, (c) Zr 3d, (d) O 1s and (e) N 1s.

copper ions. It could be speculated that a small number of defects in pz-UiO-66 itself combine with copper ions to form Zr-O-Cu bonds, leading to the above deviation in binding energy (Ma et al., 2022). In addition, the peak at 532 eV in the O 1s spectrum corresponded to the oxygen of hydroxyl groups in water molecule, which agreed with the conclusion of the infrared analysis. It was reported that the coordination sites with metal ions resulted in a shifting of the binding energy of coordination atoms to higher values, which was attributed to the electron donating/accepting ability of the metal ions (Wang et al., 1997). As depicted in Fig. 9(e), the N spectrum of pz-UiO-66-Cu showed that the N 1s binding energy of pz-UiO-66 on pyrazine nitrogen shifted from 400.2 eV to 400.8 eV after copper adsorption, indicating that this site was of vital importance for copper ion adsorption. According to the above XPS analysis, it could be concluded that pz-UiO-66 combines with Cu^{2+} ions by the coordination of pyrazine nitrogen atoms in the material and the interaction of zirconium nodes in the skeleton.

In addition, UiO-66 prepared by the same method was used as a contrast adsorbent to conduct copper adsorption experiments to prove the key role of pyrazine nitrogen atoms. In the experiments, 20 mg of the two adsorbents was separately added to 50 mL Cu^{2+} solution with a pH of 1. As shown in Fig. S5, after two h of adsorption, the adsorption capacity of UiO-66 was less than 20 mg/g, accounting for only 1/7 that of pz-UiO-66, which further indicates that the coordination of pyrazine nitrogen atoms is necessary and plays a dominant role in copper capture.

4 Conclusions

In summary, a pyrazine structured metal-organic framework was successfully synthesized by a solvothermal method, for the selective capture of copper from highly acidic solutions. pz-UiO-66 achieved effective adsorption and separation selectivity of Cu^{2+} at ultralow pH compared with other reported materials, even in mixed solutions of multiple metal ions. Furthermore, the strong Zr-O bonds and pyrazine functional groups enabled the material to maintain structural stability and adsorption capacity in highly acidic solutions. The FTIR and XPS spectra proved that the main adsorption mechanism is the coordination between pyrazine nitrogen atom and copper. Consequently, pz-UiO-66 provides a more feasible and efficient approach for the selective removal of copper from complex metal ion solutions even under highly acidic conditions.

Acknowledgements This study was financially supported by the National Natural Science Foundation of China (Nos. 52125002 and 51908270), the Natural Science Foundation of Jiangxi Province (No. 20212ACB213006), and the National Key Research and Development Program of China (No. 2019YFC1907900).

Electronic Supplementary Material Supplementary material is available in the online version of this article at https://doi.org/10.1007/s11783-023-1633-0 and is accessible for authorized users.

References

Ai K, Ruan C, Shen M, Lu L (2016). MoS_2 nanosheets with widened interlayer spacing for high-efficiency removal of mercury in aquatic systems. Advanced Functional Materials, 26(30): 5542–5549

Awual M R (2019). Novel ligand functionalized composite material for efficient copper (II) capturing from wastewater sample. Composites Part B: Engineering, 172: 387–396

Brady D C, Crowe M S, Turski M L, Hobbs G A, Yao X, Chaikuad A, Knapp S, Xiao K, Campbell S L, Thiele D J, Counter C M (2014). Copper is required for oncogenic BRAF signalling and tumorigenesis. Nature, 509(7501): 492–496

Bui N T, Kang H, Teat S J, Su G M, Pao C W, Liu Y S, Zaia E W, Guo J, Chen J L, Meihaus K R, Dun C, Mattox T M, Long J R, Fiske P, Kostecki R, Urban J J (2020). A nature-inspired hydrogen-bonded supramolecular complex for selective copper ion removal from water. Nature Communications, 11(1): 1–12

Cao Y, Xiao W, Shen G, Ji G, Zhang Y, Gao C, Han L (2019). Carbonization and ball milling on the enhancement of Pb(II) adsorption by wheat straw: competitive effects of ion exchange and precipitation. Bioresource Technology, 273: 70–76

Cavka J H, Jakobsen S, Olsbye U, Guillou N, Lamberti C, Bordiga S, Lillerud K P (2008). A new zirconium inorganic building brick forming metal organic frameworks with exceptional stability. Journal of the American Chemical Society, 130(42): 13850–13851

Chen T, Liu F, Ling C, Gao J, Xu C, Li L, Li A (2013a). Insight into highly efficient coremoval of copper and p-nitrophenol by a newly synthesized polyamine chelating resin from aqueous media: competition and enhancement effect upon site recognition. Environmental Science & Technology, 47(23): 13652–13660

Chen X, Chen A, Zhao Z, Liu X, Shi Y, Wang D (2013b). Removal of Cu from the nickel electrolysis anolyte using nickel thiocarbonate. Hydrometallurgy, 133: 106–110

Chen Y, Pan B, Li H, Zhang W, Lv L, Wu J (2010). Selective removal of Cu(II) ions by using cation-exchange resin-supported polyethyleneimine (PEI) nanoclusters. Environmental Science & Technology, 44(9): 3508–3513

Choudhary M, Kumar R, Neogi S (2020). Activated biochar derived from Opuntia ficus-indica for the efficient adsorption of malachite green dye, Cu^{2+} and Ni^{2+} from water. Journal of Hazardous Materials, 392: 122441

Daliran S, Ghazagh-Miri M, Oveisi A R, Khajeh M, Navalón S, Âlvaro M, Ghaffari-Moghaddam M, Samareh Delarami H, García H (2020). A pyridyltriazol functionalized zirconium metal-organic framework for selective and highly efficient adsorption of palladium. ACS Applied Materials & Interfaces, 12(22): 25221–25232

Demiral H, Güngör C (2016). Adsorption of copper(II) from aqueous solutions on activated carbon prepared from grape bagasse. Journal of Cleaner Production, 124: 103–113

Feng H, Li Y, Luo D, Tan G, Jiang J, Yuan H, Peng S, Qian D (2016).

Novel visible-light-responding $InVO_4$-Cu_2O-TiO_2 ternary nanoheterostructure: preparation and photocatalytic characteristics. Chinese Journal of Catalysis, 37(6): 855–862

Fitzgerald D J (1998). Safety guidelines for copper in water. The American journal of clinical nutrition, 67(5 Suppl): 1098S–1102S

Hosseinpournajjar E, Kianfar A H, Dinari M (2022). Synthesizing and characterization of Cu(II) polymer complex: application for removing heavy metals from aqueous solutions. Journal of the Iranian Chemical Society, 19(5): 1963–1977

Irving H, Williams R J P (1953). The stability of transition-metal complexes. Journal of the Chemical Society (Resumed), 3192–3210

Jiang C, Wang X, Wang G, Hao C, Li X, Li T (2019). Adsorption performance of a polysaccharide composite hydrogel based on crosslinked glucan/chitosan for heavy metal ions. Composites Part B: Engineering, 169: 45–54

Kuz'min V I, Kuz'min D V (2014). Sorption of nickel and copper from leach pulps of low-grade sulfide ores using Purolite S930 chelating resin. Hydrometallurgy, 141: 76–81

Lee S, Barin G, Ackerman C M, Muchenditsi A, Xu J, Reimer J A, Lutsenko S, Long J R, Chang C J (2016). Copper capture in a thioether-functionalized porous polymer applied to the detection of Wilson's disease. Journal of the American Chemical Society, 138(24): 7603–7609

Lin S, Kumar Reddy D H, Bediako J K, Song M H, Wei W, Kim J A, Yun Y S (2017). Effective adsorption of Pd(Ⅱ), Pt(Ⅳ) and Au(Ⅲ) by Zr(Ⅳ)-based metal-organic frameworks from strongly acidic solutions. Journal of Materials Chemistry. A, Materials for Energy and Sustainability, 5(26): 13557–13564

Ma Y, Lu W, Han X, Chen Y, da Silva I, Lee D, Sheveleva A M, Wang Z, Li J, Li W, Fan M, Xu S, Tuna F, McInnes E J L, Cheng Y, Rudić S, Manuel P, Frogley M D, Ramirez-Cuesta A J, Schröder M, Yang S (2022). Direct observation of ammonia storage in UiO-66 incorporating Cu(II) binding sites. Journal of the American Chemical Society, 144(19): 8624–8632

Marcus Y (1988). Ionic radii in aqueous solutions. Chemical Reviews, 88(8): 1475–1498

Miniyar P B, Murumkar P R, Patil P S, Barmade M A, Bothara K G (2013). Unequivocal role of pyrazine ring in medicinally important compounds: a review. Mini reviews in medicinal chemistry, 13(11): 1607–1625

Park I, Tabelin C B, Jeon S, Li X, Seno K, Ito M, Hiroyoshi N (2019). A review of recent strategies for acid mine drainage prevention and mine tailings recycling. Chemosphere, 219: 588–606

Peng Y, Huang H, Zhang Y, Kang C, Chen S, Song L, Liu D, Zhong C (2018). A versatile MOF-based trap for heavy metal ion capture and dispersion. Nature Communications, 9(1): 1–9

Shao P, Liang D, Yang L, Shi H, Xiong Z, Ding L, Yin X, Zhang K, Luo X (2020). Evaluating the adsorptivity of organo-functionalized silica nanoparticles towards heavy metals: quantitative comparison and mechanistic insight. Journal of Hazardous Materials, 387: 121676

Wang D B, Chen B H, Zhang B, Ma Y X (1997). XPS study of aroylhydrazones containing triazole and their chelates. Polyhedron, 16(15): 2625–2629

Wang L, Shi Y, Yao D, Pan H, Hou H, Chen J, Crittenden J C (2019). Cd complexation with mercapto-functionalized attapulgite (MATP): adsorption and DFT study. Chemical Engineering Journal, 366: 569–576

Wang N, Feng J, Yan W, Zhang L, Liu Y, Mu R (2022). Dual-functional sites for synergistic adsorption of Cr(VI) and Sb(V) by polyaniline-TiO_2 hydrate: adsorption behaviors, sites and mechanisms. Frontiers of Environmental Science & Engineering, 16(8): 1–14

Xie L, Yu Z, Islam S M, Shi K, Cheng Y, Yuan M, Zhao J, Sun G, Li H, Ma S, Kanatzidis M G (2018). Remarkable acid stability of polypyrrole-MoS_4: a highly selective and efficient scavenger of heavy metals over a wide pH range. Advanced Functional Materials, 28(20): 1800502

Xu M, Meng S S, Liang H, Gu Z Y (2020). A metal-organic framework with tunable exposed facets as a high-affinity artificial receptor for enzyme inhibition. Inorganic Chemistry Frontiers, 7(19): 3687–3694

Yao Z, Shao P, Fang D, Shao J, Li D, Liu L, Huang Y, Yu Z, Yang L, Yu K, Luo X (2022). Thiol-rich, porous carbon for the efficient capture of silver: understanding the relationship between the surface groups and transformation pathways of silver. Chemical Engineering Journal, 427: 131470

Yu H, Shao P, Fang L, Pei J, Ding L, Pavlostathis S G, Luo X (2019). Palladium ion-imprinted polymers with PHEMA polymer brushes: role of grafting polymerization degree in anti-interference. Chemical Engineering Journal, 359: 176–185

Zhang X, Tong S, Huang D, Liu Z, Shao B, Liang Q, Wu T, Pan Y, Huang J, Liu Y, Cheng M, Chen M (2021). Recent advances of Zr based metal organic frameworks photocatalysis: energy production and environmental remediation. Coordination Chemistry Reviews, 448: 214177

Zhang Y, Xie Z, Wang Z, Feng X, Wang Y, Wu A (2016). Unveiling the adsorption mechanism of zeolitic imidazolate framework-8 with high efficiency for removal of copper ions from aqueous solutions. Dalton Transactions, 45(32): 12653–12660